


Article

A Facile Method to Fabricate Al₂O₃-SiO₂ Aerogels with Low Shrinkage up to 1200 °C

Yulin Tian, Xiaodong Wang *, Yu Wu, Xiaoxue Zhang, Chun Li, Yijun Wang and Jun Shen *

Shanghai Key Laboratory of Special Artificial Microstructure Materials and Technology, School of Physics Science and Engineering, Tongji University, Shanghai 200092, China

* Correspondence: xiaodong_wang@tongji.edu.cn (X.W.); shenjun67@tongji.edu.cn (J.S.)

Abstract: Monolithic Al₂O₃-SiO₂ composite aerogels were synthesized by using inexpensive aluminum chloride hexahydrate (AlCl₃·6H₂O) and tetraethyl orthosilicate (TEOS). By adjusting the molar ratio of Al and Si, the best ratio of high-temperature resistance was found. The resultant aerogels (Al:Si = 9:1) exhibit high thermal performance, which can be identified by the low linear shrinkage of 5% and high specific surface area (SSA) of 283 m²/g at 1200 °C. Alumina in these aerogels mainly exists in the boehmite phase and gradually transforms into the θ-Al₂O₃ phase in the process of heating to 1200 °C. No α-Al₂O₃ is detected in the heating process. These Al₂O₃-SiO₂ composite aerogels are derived from a simple, low-priced and safe method. With their high thermal performance, these aerogels will have a wide application in high-temperature field.

Keywords: Al₂O₃-SiO₂ composite aerogels; high-temperature performance; high specific surface area

1. Introduction

Alumina aerogels are unique nanoporous materials with low thermal conductivity, high specific surface area and high temperature performance [1–6]. Due to the excellent performance at high temperature, alumina aerogels were considered to be high-temperature insulation materials and high-temperature catalysts. In addition, alumina aerogels were used as catalysts for the reactions of NO reduction, CO oxidation, and hydrocarbons oxidation. It should be noted that alumina aerogels retain a high specific surface area up to 800 °C, which is very important for catalytic reaction since most of them occur at elevated temperatures [7–9]. However, the sintering and brittleness of alumina aerogels at high temperatures have always been important factors hindering their practical application [10–13]. With the development of thermal insulation materials, it was found that the alumina aerogels obtained by doping and composite have greatly improved high-temperature thermal stability, which gives the alumina-based aerogels better application prospects [14–16].

Alumina aerogels usually use aluminum alkoxides or aluminum inorganic salts as precursors, adding Si, Zr, Ti, Y and La to improve their high-temperature thermal stability. The precursors of alumina aerogels are mainly divided into alumina alkoxides such as sec-butoxide (ASB) or isopropoxide (AIP), and alumina inorganic salts such as aluminum chloride (AlCl₃·6H₂O) or aluminum nitrate (Al(NO₃)₃·9H₂O) [17]. For the alumina alkoxides, Yang et al. prepared silica-doped alumina aerogels via ASB and TEOS as precursors by rapid supercritical drying, which exhibited a stable γ-Al₂O₃ phase and a high SSA of 146 m²/g at 1200 °C when the silica content was in the range of 10.6–13.1 wt% [18]. Wang et al. modified the alumina aerogels derived from ASB using trimethylethoxysilane (TMEO), the modified samples exhibited no shrinkage, a θ-Al₂O₃ phase and a high SSA of 147 m²/g at 1200 °C [19]. Zhang et al. synthesized alumina aerogels from AlCl₃·6H₂O using acetoacetic-grafted polyvinyl alcohol as a template; the samples possessed high elastic modulus of 8.81 MPa, a γ-Al₂O₃ phase and a high SSA of 143 m²/g at 1000 °C [20]. Although the alumina aerogels derived from alumina alkoxides exhibited good thermal



Citation: Tian, Y.; Wang, X.; Wu, Y.; Zhang, X.; Li, C.; Wang, Y.; Shen, J. A Facile Method to Fabricate Al₂O₃-SiO₂ Aerogels with Low Shrinkage up to 1200 °C. *Molecules* **2023**, *28*, 2743. <https://doi.org/10.3390/molecules28062743>

Academic Editor: Xiongfei Zhang

Received: 23 December 2022

Revised: 12 March 2023

Accepted: 13 March 2023

Published: 17 March 2023



Copyright: © 2023 by the authors. Licensee MDPI, Basel, Switzerland. This article is an open access article distributed under the terms and conditions of the Creative Commons Attribution (CC BY) license (<https://creativecommons.org/licenses/by/4.0/>).

performance, the alumina alkoxides demonstrate ultrahigh reactivity, complex chemical reaction pathways, unacceptable price and biological safety issues, which become huge obstacles to high-temperature applications [21]. The method of using inorganic aluminum salts as the precursor to prepare alumina aerogels is simple, and the precursor cost is low, so it has a better industrial application value. The existing research results show that introducing SiO₂ into alumina aerogels is an effective and economical way to improve the high-temperature performance [22,23].

In this work, we applied AlCl₃·6H₂O and TEOS to prepare Al₂O₃-SiO₂ composite aerogels using the propylene oxide (PO) addition method. The method uses PO as a proton-trapping agent to promote the multistage hydrolysis of Al³⁺ and form a stable three-dimensional network structure [24]. In general, adding SiO₂ into alumina aerogels will enhance the thermal stability of the gel at high temperature. However, the introduction of too much SiO₂ may reduce the high-temperature thermal performance of alumina aerogels. In order to find out the range of SiO₂ content, which can enhance the performance of alumina aerogels, we prepared several groups of samples from low to high SiO₂ content. Among them, samples with lower SiO₂ content showed better thermal stability than pure alumina aerogels, while samples with higher SiO₂ content experienced reduced high-temperature performance. For samples with low SiO₂ content, the introduction of SiO₂ enhances the skeleton strength and mechanical strength of alumina aerogels and also suppresses the phase transition from θ-Al₂O₃ to α-Al₂O₃, thus improving the thermal properties [25]. This work studied the influence of silicon content on the high-temperature performance of aerogels in Al₂O₃-SiO₂ composite aerogels and found the range of SiO₂ that provides a positive effect. These findings have a guiding role in the subsequent Al₂O₃-SiO₂ composite process. These Al₂O₃-SiO₂ composite aerogels with high thermal performance derived from a simple, low-priced and safe method have a wide application in the high-temperature field.

2. Results

2.1. Synthesis of Al₂O₃-SiO₂ Aerogels

Al₂O₃-SiO₂ composite aerogels were prepared by the PO addition method and ethanol supercritical drying process [24]. AlCl₃·6H₂O and TEOS were dissolved in 84 mL of ethanol aqueous solution (the volume ratio of ethanol to water was 7:3), and 35 mL of PO was added after stirring for ten minutes. The total amount of AlCl₃·6H₂O and TEOS was 0.05 mol. The samples were denoted as AS0, AS1, AS2, AS3, AS4 and AS5 according to the molar ratios of TEOS to AlCl₃·6H₂O = 0:10, 1:9, 2:8, 3:7, 4:6 and 5:5, respectively. After aging for one day, the solvent of wet gel was displaced with fresh ethanol 7 times (12 h for each time). The aerogels were finally obtained by the ethanol supercritical drying process with temperature of 265 °C and pressure of 10 MPa. Then the samples were heat-treated at 600, 800, 1000 and 1200 °C for 1 h gradually, and the corresponding samples were denoted by adding the heat treatment as a suffix (e.g., AS0-600 and AS1-1200).

2.2. Macro Morphology and Properties at Room Temperature

Figure 1 shows the macroscopic morphology of Al₂O₃-SiO₂ composite aerogels. With the increase in SiO₂ content, the color of these aerogels gradually deepened, and the sample cracked when the molar ratio of Si to Al was 1:1. The density, linear shrinkage and thermal conductivity of the aerogels are shown in Table 1. The linear shrinkage here refers to the reduction in diameter from wet gel to aerogel. The linear shrinkage of AS1 and AS2 is lower than that of AS0, which indicates that the adding of a small amount of SiO₂ improves the thermal stability of the aerogels. The linear shrinkage of AS3, AS4 and AS5 is significantly higher than that of AS0, which indicates the excessive adding of SiO₂ will not only destroy the formability of alumina aerogel bulks but also reduce their thermal stability. The thermal conductivities of AS samples at room temperature (20 °C) are between 0.033 and 0.037 W/m·K, indicating that AS samples have excellent thermal insulation ability.

2.3. Shrinkage after Different Heating Temperatures

Figure 2a shows the linear shrinkage of AS samples under high-temperature heat treatment, which can represent their high-temperature thermal stability. Figure 2b shows the physical photos of AS1 sample before and after treatment at 1200 °C. Compared with AS0, the linear shrinkage of AS1 and AS2 between 1000 °C and 1200 °C is significantly reduced, which indicates that adding a small amount of silicon can effectively improve the high-temperature thermal stability of alumina-based aerogels. The high-temperature linear shrinkage of AS4 and AS5 is significantly larger than that of AS0, which is due to the introduction of a large amount of SiO₂, and the SiO₂ starts to agglomerate at a high temperature above 600 °C. Among them, the linear shrinkage of AS1 after heat treatment at 1200 °C is only 5%, which shows excellent thermal stability at high temperature.

According to the different amount of silica, the AS samples transformed to γ -, δ -, θ -Al₂O₃ and mullite [15,25]. In the process of sol gel, silica is basically amorphous, and alumina exists as the boehmite phase [21]. Finally, SiO₂ is introduced to form -Si-O-Al- bonds, and the Si distributed in the alumina lattice will inhibit the phase transition [26]. Therefore, increasing the uniform distribution of SiO₂ in alumina aerogels is conducive to improving the thermal stability of alumina aerogels.

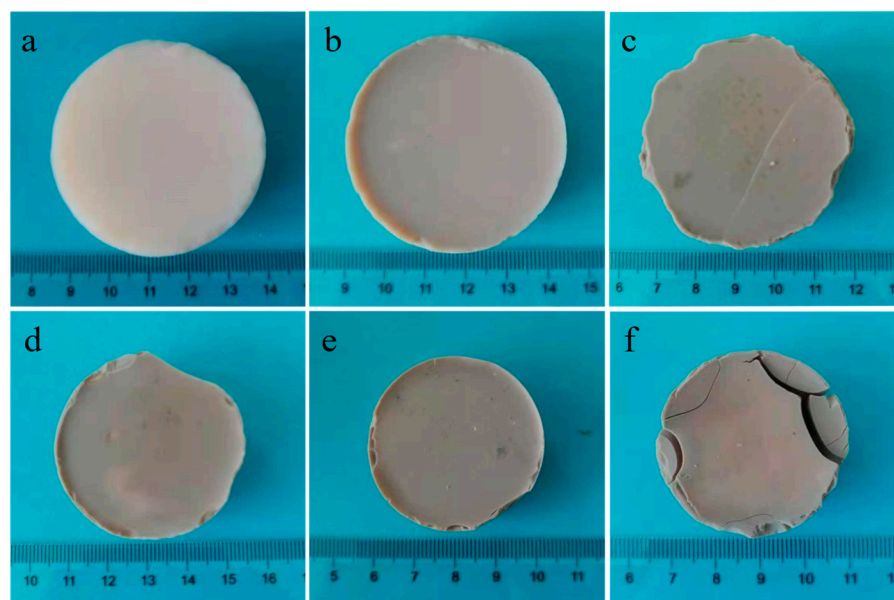


Figure 1. Digital photos of Al₂O₃-SiO₂ composite aerogels (a) AS0, (b) AS1, (c) AS2, (d) AS3, (e) AS4 and (f) AS5.

Table 1. Density, liner shrinkage and thermal conductivity (20 °C) of the AS samples.

Sample	Density (mg/cm ³)	Liner Shrinkage (%)	Thermal Conductivity (W/m·K)
AS0	32	12	0.033
AS1	42	8	0.035
AS2	40	10	0.036
AS3	62	15	0.035
AS4	83	23	0.037
AS5	96	23	0.036

2.4. Micromorphology at Different Temperatures

Figure 3 shows the microstructure of AS0 from 20 to 1200 °C. As shown in Figure 3a–e, the alumina aerogel AS0 exhibits a fibrous three-dimensional network porous structure, which is mainly composed of lamellar and strip nanoparticles. With the increment of heat

treatment temperature, there is no obvious particle aggregation and structure collapse, and AS0 still maintains the nanoporous structure. As the temperature rises to 1200 °C, the nanoporous structure of AS0 does not change, but it can be seen that the voids are significantly smaller and the structure is more compact. Figure 4 shows the microstructure of AS1 from 20 to 1200 °C. Compared with the AS0 sample, the structure of AS1 is obviously different and mainly composed of larger lamellar and strip nanoparticles. After 1200 °C heat treatment, the structure of AS1 does not change significantly. It can be considered that the introduction of SiO₂ makes the microstructure of alumina aerogels coarser. At the same time, the introduction of SiO₂ can reduce the hydroxyl groups on the surface of Al₂O₃, prevent the dehydroxylation reaction and thus inhibit its phase transformation at high temperature [27,28]. In addition, SiO₂ can also reduce the contact between Al₂O₃ particles and effectively control the surface/bulk diffusion, thus improving the temperature resistance of Al₂O₃ aerogel [29].

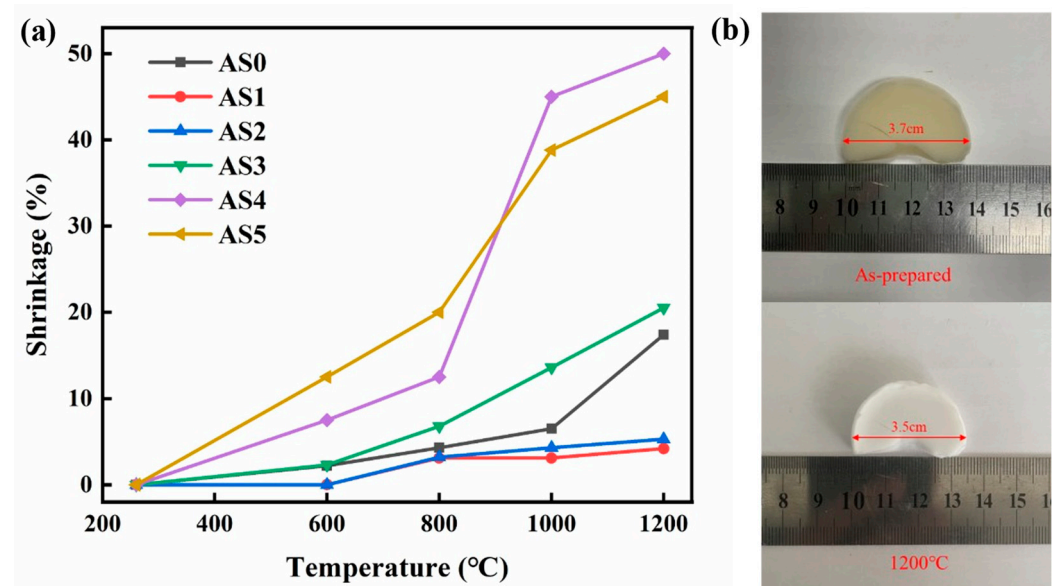


Figure 2. (a) The linear shrinkage of AS samples after heat treatment; (b) digital photos of AS1 before and after 1200 °C heat treatment.

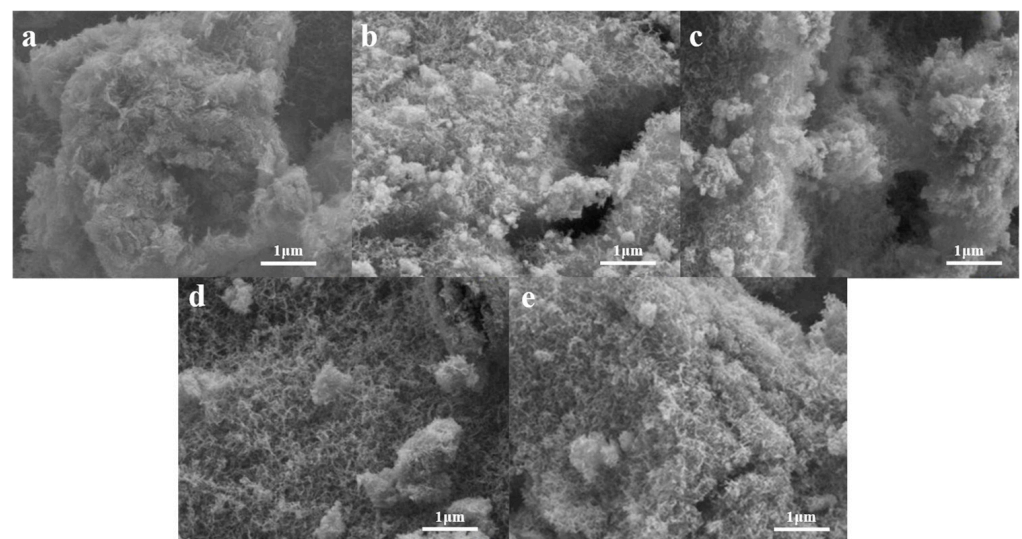


Figure 3. Scanning electron microscopy (SEM) images of AS0 after heat treatment from 20 to 1200 °C: (a) AS0-20, (b) AS0-600, (c) AS0-800, (d) AS0-1000, (e) AS0-1200.

2.5. Variation of Chemical Composition at Different Temperatures

Figure 5a, b show the variation in chemical bonds of the AS0 and AS1 samples after heat treatment from 20 to 1200 °C. As shown in Figure 5a, AS0 mainly presents as the boehmite phase at room temperature after the supercritical drying process. The peaks at 3449 and 1634 cm^{-1} correspond to the stretching and bending vibrations of the physically adsorbed water, respectively. The bands at 1075 cm^{-1} correspond to the vibration modes of Al-OH in the boehmite crystal phase. The bands at 885, 780, 620 and 489 cm^{-1} also correspond to the vibration mode of Al-O-Al and torsional vibration, stretching vibration and bending vibration of Al-O in the boehmite crystal [30–32], respectively. When the heat-treated temperature rises above 600 °C, the characteristic infrared peaks corresponding to the boehmite phase of AS0 all disappear, indicating that the crystal phase transition of alumina aerogels has taken place. All these absorption bands of the pseudo-boehmite structure disappear after heat treatment at 600 °C, followed by the emergence of broad adsorption bands in the low-frequency region of 500–900 cm^{-1} [30–32]. With the further increment of temperature, the absorption band of Al_2O_3 aerogel becomes wider, indicating that its crystallinity is improved. After heat treatment at 800 °C, there are two wide absorption peaks at 574 and 829 cm^{-1} , which correspond to the vibration modes of Al-O in the $\theta\text{-Al}_2\text{O}_3$ phase, indicating the appearance of a partial $\theta\text{-Al}_2\text{O}_3$ crystal phase. In the process of heat treatment, the characteristic absorption peaks of 448 and 637 cm^{-1} corresponding to $\alpha\text{-Al}_2\text{O}_3$ do not appear all the time, indicating that there is no $\alpha\text{-Al}_2\text{O}_3$ crystal phase, and the alumina AS0 sample shows good thermal stability [30]. As shown in Figure 5b, the $\text{Al}_2\text{O}_3\text{-SiO}_2$ aerogel AS1 also presents as the boehmite crystal phase at room temperature. When the heat-treated temperature rises to 600 °C, the characteristic infrared peaks corresponding to the boehmite phase of AS1 also disappear, and a wide absorption band corresponding to the $\gamma\text{-Al}_2\text{O}_3$ crystal appears. The infrared peaks of AS1 hardly change in the subsequent heating process, indicating that the addition of SiO_2 effectively inhibits the phase transition of alumina aerogels and keeps the alumina aerogels intact, which is consistent with the previous linear shrinkage of only 5% at 1200 °C.

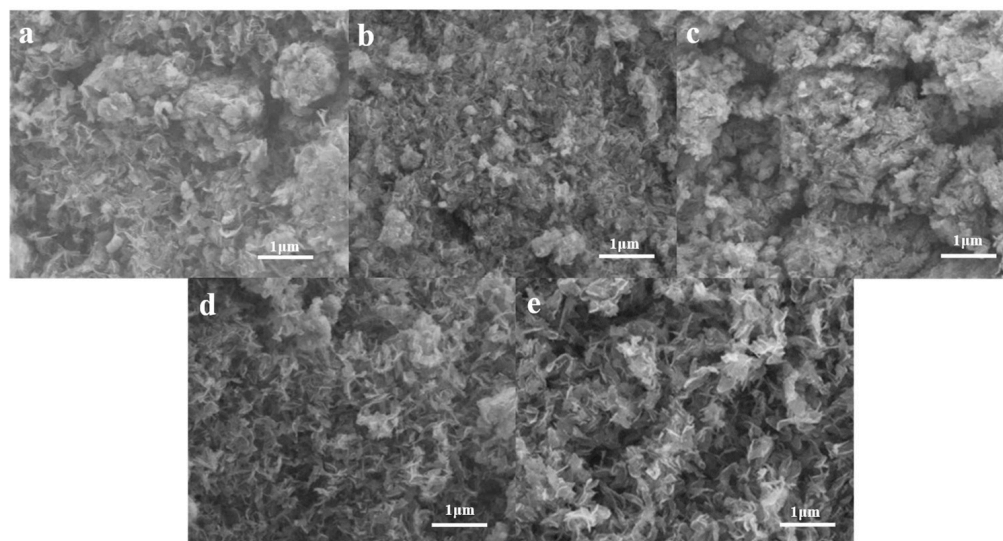


Figure 4. Scanning electron microscopy (SEM) images of AS1 after heat treatment from 20 to 1200 °C: (a) AS1-20, (b) AS1-600, (c) AS1-800, (d) AS1-1000, (e) AS1-1200.

Figure 5c reflects the changes of crystal structure of alumina aerogel AS0 after heat treatment from 20 to 1200 °C. The AS0 sample shows its boehmite phase at room temperature. The sharp peaks at $2\theta = 28^\circ, 38^\circ, 49^\circ, 65^\circ$ and 72° correspond to the characteristic diffraction of boehmite (120), (031), (200), (002) and (251) crystal planes [33]. After heat treatment at 600 °C, AS0 transforms from the boehmite phase to the $\gamma\text{-Al}_2\text{O}_3$ phase. The peaks at $2\theta = 46^\circ$ and 66° correspond to the diffraction of $\gamma\text{-Al}_2\text{O}_3$ (400) and (440) crystal

planes, respectively [34]. However, the peaks of other γ - Al_2O_3 crystal planes do not appear, indicating that the crystallinity of the γ - Al_2O_3 phase is low. After heat treatment at 800 °C, the peaks of the γ - Al_2O_3 crystal phase are more obvious, and new weak peaks at $2\theta = 37^\circ$ and 39° appear, corresponding to the diffraction peaks of γ - Al_2O_3 (311) and (222) crystal planes, respectively [35]. After heat treatment at 1000 °C, γ - Al_2O_3 transforms into the θ - Al_2O_3 phase, and the peaks at $2\theta = 39^\circ$, 45° and 67° correspond to the diffraction of θ - Al_2O_3 (104), (21-1) and (215), respectively. After heat treatment at 1200 °C, the characteristic diffraction peaks of the θ - Al_2O_3 phase become stronger, and a new peak at $2\theta = 33^\circ$ that corresponds to the (20-2) crystal plane diffraction of the θ - Al_2O_3 phase appears, indicating that AS0 exhibits a stable θ - Al_2O_3 crystal phase and does not transform into an α - Al_2O_3 phase at 1200 °C. Figure 5d reflects the changes of crystal phase of Al_2O_3 - SiO_2 composite aerogels AS1 after heat treatment at different temperatures. The AS1 sample also shows the same boehmite crystal structure and has five characteristic diffraction peaks at $2\theta = 28^\circ$, 38° , 49° , 65° and 72° at room temperature. After heat treatment at 600 and 800 °C, AS1 also transforms into the γ - Al_2O_3 phase, but its characteristic diffraction peaks only appear at $2\theta = 66^\circ$, indicating the overall crystallinity is very low. After heat treatment at 1000 and 1200 °C, AS1 transforms into the θ - Al_2O_3 crystal phase, and the characteristic diffraction peak is also reduced; only peaks at $2\theta = 45^\circ$ and 67° appear, which indicates that the addition of SiO_2 can effectively hinder the crystal transition of alumina aerogels and improve their thermal stability significantly.

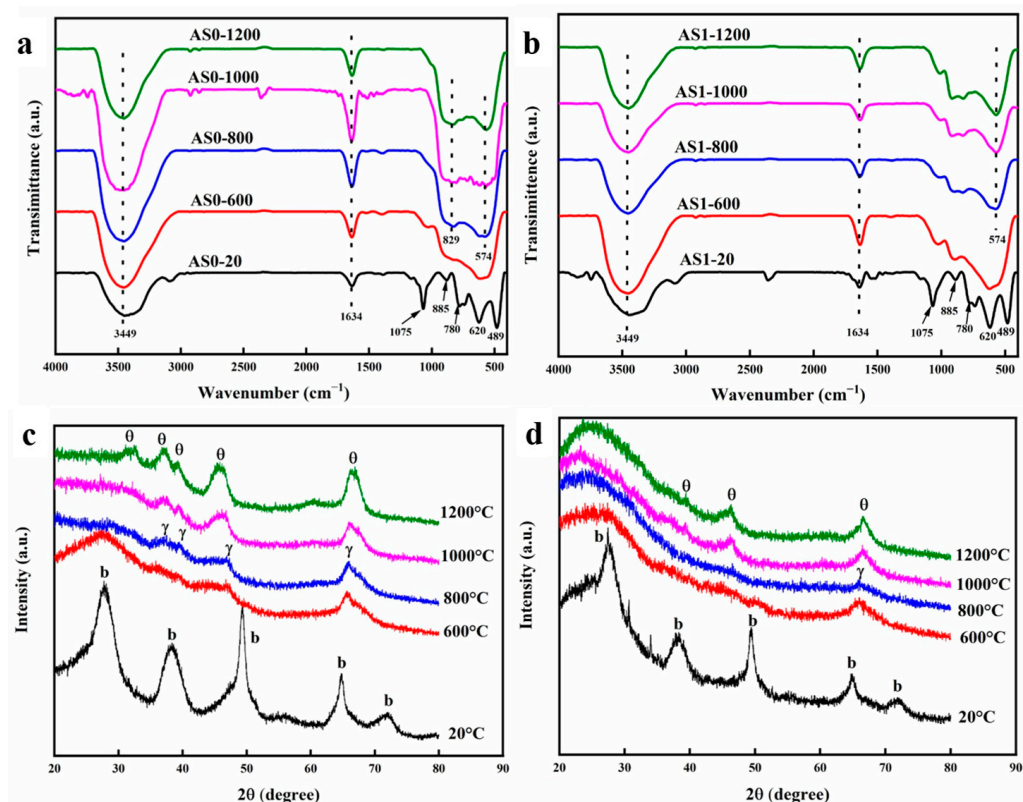


Figure 5. Fourier transform infrared spectrometer (FTIR) of the (a) AS0 and (b) AS1 after heat treatment from 20 to 1200 °C; X-ray diffraction (XRD) pattern of (c) AS0 and (d) AS1 after heat treatment from 20 to 1200 °C.

Figure 6a reflects the infrared absorption peaks of all AS samples after calcination at 1200 °C for 1 h. The absorption peaks at 3449 and 1634 cm^{-1} correspond to the stretching and bending vibration of physically adsorbed water, respectively. The bands at 570 and 830 cm^{-1} correspond to the vibration mode of Al-O in the θ - Al_2O_3 phase. With the increment of the Si/Al molar ratio, AS samples exhibit different FTIR spectra. After heat treatment at 1200 °C, AS samples at 570 and 830 cm^{-1} also contain weak absorption peaks,

indicating that they are mainly in the θ - Al_2O_3 crystal phase, but the crystallization degree is lower than that of AL samples. In addition, the bands at 467 and 1094 cm^{-1} in AS4 and AS5 correspond to the vibration modes of Si-O-Si, while these absorption peaks do not appear in the samples with low silica content such as AS1, AS2 and AS3, indicating that silicon mainly exists in the form of Al-O-Si in these samples, which is helpful to improving the thermal stability of alumina aerogels.

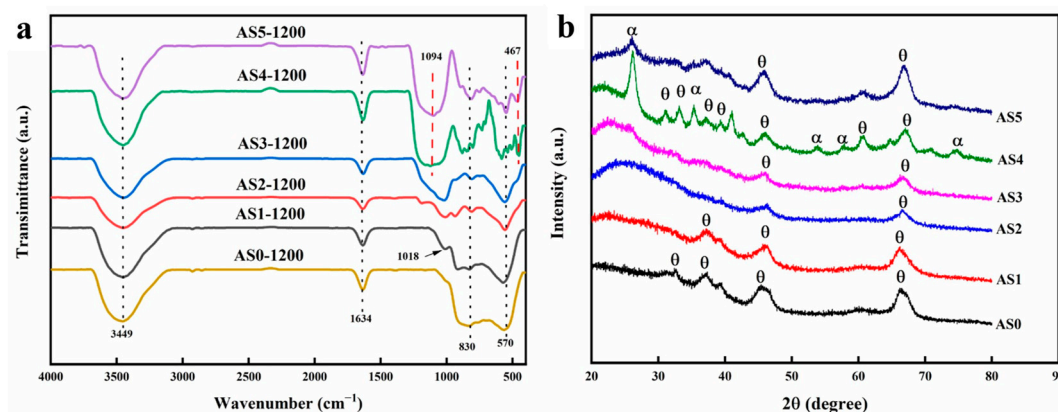


Figure 6. Fourier transform infrared spectrometer (FTIR) (a) and X-ray diffraction (XRD) pattern (b) of all AS samples after heat treatment at $1200\text{ }^{\circ}\text{C}$.

Figure 6b demonstrates the crystal phase of all the AS samples after heat treatment at $1200\text{ }^{\circ}\text{C}$. For Al_2O_3 - SiO_2 composite aerogels, AS1, AS2 and AS3 only show a θ - Al_2O_3 crystal phase, but the crystallinity is lower than that of AS0, which indicates that the introduction of SiO_2 effectively hinders the crystal phase transition of alumina aerogels. However, too much SiO_2 exhibits adverse effects. In addition to the characteristic diffraction peaks of the θ - Al_2O_3 crystal phase, the AS4 sample also has the characteristic diffraction peaks of α - Al_2O_3 at $2\theta = 26^{\circ}, 35^{\circ}, 53^{\circ}$ and 58° , which correspond to α - Al_2O_3 (012), (104), (113) and (024) crystal planes, respectively [11,27]. Therefore, the AS4 sample presents a mixed crystal phase of θ - Al_2O_3 and α - Al_2O_3 , indicating that the introduction of too much SiO_2 amount reduces the thermal stability of alumina aerogels. AS5 also presents a mixed crystal phase of θ - Al_2O_3 and α - Al_2O_3 , but the crystallinity is lower than that of AS4.

2.6. SSA and Pore Size Distribution at Different Temperatures

Figure 7a–d show the N_2 adsorption–desorption curves and pore size distribution of AS0 and AS1 samples after heat treatment from 20 to $1200\text{ }^{\circ}\text{C}$. It is found that the N_2 adsorption–desorption curves of the two samples belong to Type-IV isotherms and the Type-H3 hysteresis loop, which indicates that the two samples mainly possess mesoporous structures formed by the accumulation of nanoparticles [36]. As shown in Figure 7b,d, AS0 and AS1 samples have similar pore size distribution and changing rules. As shown in Figure 8a, in the heating process from 20 to $1200\text{ }^{\circ}\text{C}$, the specific surface area (SSA) of both AS0 and AS1 gradually increases at first and then decreases slowly, which is caused by the removal of organic groups and the formation of some new mesoporous structure. This point can be identified by the change of sample color and the disappearance of organic groups during the heat treatment. By comparing AS0 and AS1 samples, it is found that AS0 has higher SSA at room temperature, which is mainly due to its lower density and higher porosity. However, in the process of heat treatment, although the SSA of the two types of samples decreases gradually after $600\text{ }^{\circ}\text{C}$, the reduction rate of AS1 is slow, and the SSA of AS1 exceeds that of AS0 after $1000\text{ }^{\circ}\text{C}$, which fully shows the promotion effect of silica composite on alumina aerogels to maintain nanoporous structure at high temperature.

Figure 7e,f reflect the N_2 adsorption–desorption curves and pore size distribution of all the AS samples after heat treatment at $1200\text{ }^{\circ}\text{C}$. It is found that the N_2 adsorption–desorption curves of both samples still maintain Type-IV isotherms and the Type-H3

hysteresis loop. The average pore size of AS0, AS1, AS2 and AS3 is distributed around 30 nm, while the average pore size of AS4 and AS5 decreases rapidly to 20 nm, indicating the sinter of their nanoporous structure. As shown in Figure 8b, the SSA of all AS samples increases at first and then decreases rapidly with the increment of SiO₂ content, indicating that the appropriate composite amount of SiO₂ can effectively improve the thermal stability of alumina aerogels. The SSAs of AS2 and AS3 with low SiO₂ content are up to 283 and 282 m²/g, respectively. However, when the composite amount of SiO₂ exceeds 30%, the SSA of the SiO₂-Al₂O₃ aerogels decreases rapidly, because silica gradually becomes the main skeleton of composite aerogels with low thermal stability, which will inevitably cause the collapse of the skeleton structure at high temperature.

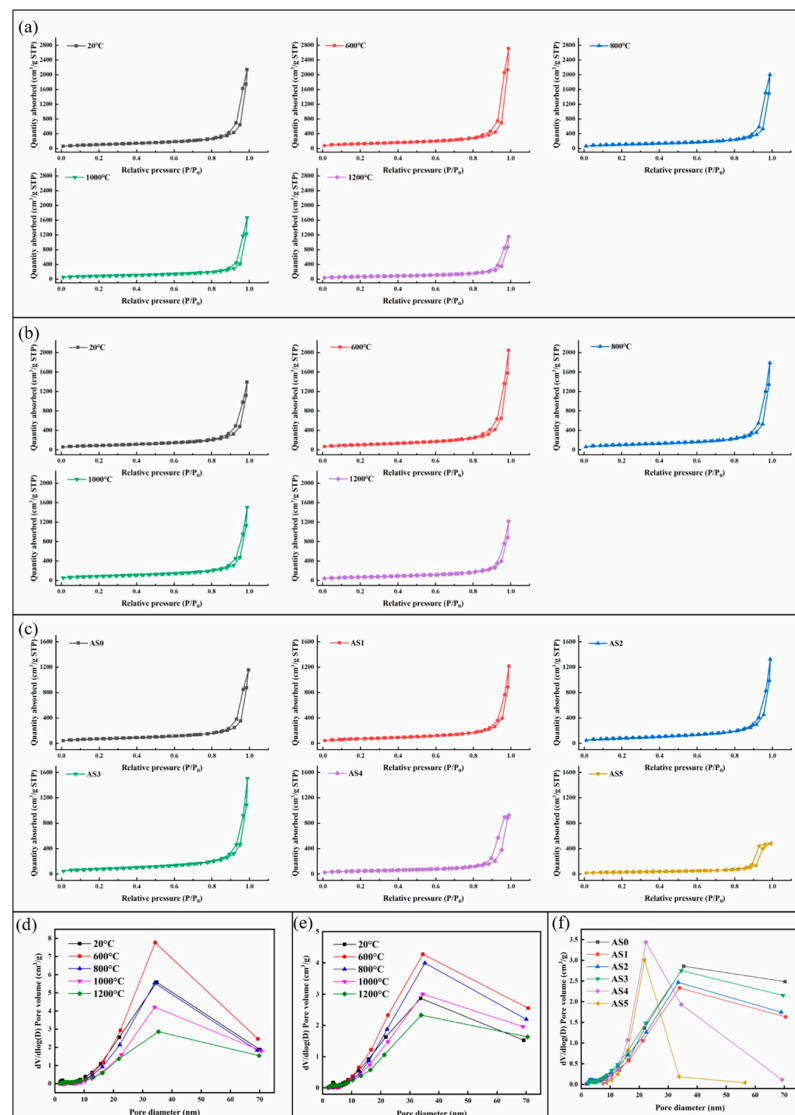


Figure 7. N₂ adsorption–desorption isotherms of (a) AS0, (b) AS1 and (c) all AS samples after heat treatment at 1200 °C; pore size distribution of (d) AS0, (e) AS1 and (f) all AS samples after heat treatment at 1200 °C.

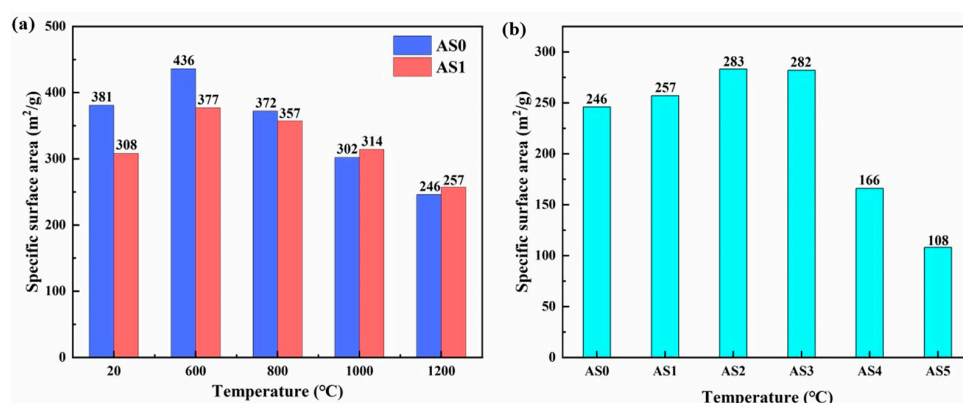


Figure 8. Specific surface area (SSA) of (a) AS0 and AS1 samples after heat treatment from 20 to 1200 °C and (b) all AS samples after heat treatment at 1200 °C.

Table 2 shows the average pore size and pore volume of all AS samples. The pore size and pore volume of AS0 and AS1 increase first and then decrease with the increase in temperature, which is consistent with the trend of pore size distribution and specific surface area. In the process of heating the samples from 20 to 600 °C, as the by-products of the reaction and the organic matter attached to the skeleton surface are decomposed at high temperature, leaving more pores, the pore size of AS sample increases, and the specific surface area also increases. In this process, the samples gradually change from grayish brown and brownish yellow to white. Then with the increase in temperature, the SiO₂ in the samples are sintered, the alumina crystal phase is transformed, the pore size is gradually reduced, the pore volume shrinks and the specific surface area is also gradually reduced. Observing the performance of all AS samples at 1200 °C, it can be seen that AS4 and AS5 are significantly sintered at high temperature due to high SiO₂ content, and the pore size is significantly reduced. This result is consistent with the data shown above and shows that in the Al₂O₃-SiO₂ composite aerogels, if the Si:Al exceeds 3:7, the high-temperature performance of the aerogels will be seriously reduced.

Table 2. Average pore diameter and pore volume of AS samples.

Sample	Pore Volume (cm ³ /g)	Pore Diameter (nm)	Sample	Pore Volume (cm ³ /g)	Pore Diameter (nm)	Sample	Pore Volume (cm ³ /g)	Pore Diameter (nm)
AS0-20	3.31	31.0	AS1-20	2.15	28.3	AS0-1200	2.30	33.0
AS0-600	4.20	34.2	AS1-600	3.17	33.4	AS1-1200	1.89	29.9
AS0-800	3.09	33.4	AS1-800	2.75	33.6	AS2-1200	2.05	28.8
AS0-1000	2.57	35.6	AS1-1000	2.31	31.8	AS3-1200	2.33	31.5
AS0-1200	2.30	33.0	AS1-1200	1.89	29.9	AS4-1200	1.44	24.6
						AS5-1200	0.75	21.0

3. Experimental

3.1. Materials

Tetraethyl orthosilicate (TEOS), aluminum chloride hexahydrate (AlCl₃·6H₂O), ethanol and propylene oxide (PO) were purchased from Sinopharm Chemical Reagent Corporation (Shanghai, China). Deionized water was applied in all experiments. All reagents were analytical grade and were used as received without further purification.

3.2. Characterization

The linear shrinkage was calculated depending on the change in the cylinder diameters of the aerogels with an increment in temperature. The samples compared were the as-prepared aerogels derived from the supercritical drying process without any treatment. Bulk density was determined by the mass and volume of regular cylinders. The surface

morphology was observed by scanning electron microscopy (ZEISS Sigma 300, Oberkochen, Germany). The chemical groups that remained in the samples were investigated by a Fourier transform infrared spectrometer (FTIR, TENSOR27, Bruker, Karlsruhe, Germany), and all samples were dispersed in dry KBr and pressed into a semitransparent slice for FTIR characterization. The crystal phase of the aerogels was analyzed by powder X-ray diffraction (XRD) with a Rigata/max-C diffractometer using Cu-K α radiation at a scanning speed of 2°/min within the 2 θ range of 10–90° (Rigaku Ultima IV, Tokyo, Japan). The thermal conductivities were measured by a hotdisk thermal constant analyzer (TPS2500, Sweden). The specific surface area (SSA) and pore size distributions of the samples were obtained by a N₂ adsorption analyzer (ASAP2460, Shanghai, China). The surface areas and pore sizes were determined by the Brunauer–Emmett–Teller (BET) and Barrett–Joyner–Halenda (BJH) methods.

4. Conclusions

In this work, we reduced the molar ratio of alumina to silica gradually from 10:0 to 5:5 to study the influence of the introduction of SiO₂ on the structure and properties of alumina aerogels. The Al₂O₃-SiO₂ composite aerogels were monolithic, dark brown and opaque without obvious cracks, indicating that they contained some organic groups, which would be gradually removed in the heat treatment process, and the color of the samples eventually turns white. The AS samples with low SiO₂ content (10~20%) showed excellent thermal performance, which can be identified by their low linear shrinkage of 5%, stable θ -Al₂O₃ phase and high SSA of 283 m²/g at 1200 °C, because SiO₂ can hinder the phase transition and collapse of structure effectively. However, when the SiO₂ content exceeded 30%, the SiO₂-Al₂O₃ aerogels appeared in the α -Al₂O₃ phase, leading to a sintering phenomenon and a big loss of SSA to 108 m²/g at 1200 °C. Although the skeleton structure of the composite samples was mainly Al₂O₃, there were some silica particles and -Al-O-Si- chemical bonds. The -Al-O-Si- bonds entered into the crystal structure of alumina aerogels and hindered their crystal phase transition. These Al₂O₃-SiO₂ composite aerogels derived from a simple, low-priced and safe method with high thermal performance have a wide application in the high-temperature field.

Author Contributions: Conceptualization, Y.T. and Y.W. (Yu Wu); Data curation, Y.W. (Yijun Wang); Formal analysis, Y.T.; Investigation, X.Z. and C.L.; Methodology, X.W.; Writing—original draft, Y.T.; Writing—review and editing, X.W. and J.S. All authors have read and agreed to the published version of the manuscript.

Funding: This research was funded by the National Key Research and Development Program of China, grant number 2017YFA0204600.

Institutional Review Board Statement: Not applicable.

Informed Consent Statement: Not applicable.

Data Availability Statement: All data are included in the article.

Conflicts of Interest: The authors declare no conflict of interest.

Sample Availability: Not applicable.

References

1. Peng, F.; Jiang, Y.G.; Feng, J.; Cai, H.F.; Feng, J.Z.; Li, L.J. Research Progress on Alumina Aerogel Composites for High-temperature Thermal Insulation. *J. Inorg. Mater.* **2021**, *36*, 673–684. [[CrossRef](#)]
2. Despetis, F.; Calas-Etienne, S.; Etienne, P. Slow crack growth in silica aerogels: A review. *J. Sol-Gel Sci. Technol.* **2019**, *90*, 20–27. [[CrossRef](#)]
3. Zhang, Z.; Wang, X.; Wu, Y.; Zou, W.; Wu, X.; Shen, J. Aerogels and Their Applications—A Short Review. *J. Chin. Ceram. Soc.* **2018**, *46*, 1426–1446.
4. Randall, J.P.; Meador MA, B.; Jana, S.C. Tailoring Mechanical Properties of Aerogels for Aerospace Applications. *ACS Appl. Mater. Inter.* **2011**, *3*, 613–626. [[CrossRef](#)]

5. Wang, X.; Zhang, Z.; Wang, Y.; Malfait, W.J.; Zhao, S.; Tian, Y.; Liu, T.; Zhang, X.; Du, A.; Shen, J. Flexible, high-temperature-resistant silica-polymer aerogel hybrids by templating polymethylsilsesquioxane microstructure with trace polyimide. *Adv. Compos. Hybrid Mater.* **2023**, *6*, 32. [[CrossRef](#)]
6. Wang, X.; Tian, Y.; Yu, C.; Liu, L.; Zhang, Z.; Wu, Y.; Shen, J. Organic/inorganic double-precursor cross-linked alumina aerogel with high specific surface area and high-temperature resistance. *Ceram. Int.* **2022**, *48*, 17261–17269. [[CrossRef](#)]
7. Bono, M.S.; Anderson, A.M.; Carroll, M.K. Alumina aerogels prepared via rapid supercritical extraction. *J. Sol-Gel Sci. Technol.* **2010**, *53*, 216–226. [[CrossRef](#)]
8. Juhl, S.J.; Dunn, N.J.; Carroll, M.K.; Anderson, A.M.; Bruno, B.A.; Madero, J.E.; Bono, M.S. Epoxide-assisted alumina aerogels by rapid supercritical extraction. *J. Non-Cryst. Solids* **2015**, *426*, 141–149. [[CrossRef](#)]
9. Zou, W.; Wang, X.; Wu, Y.; Zu, G.; Zou, L.; Zhang, R.; Yao, X.; Shen, J. Highly thermally stable alumina-based aerogels modified by partially hydrolyzed aluminum tri-sec-butoxide. *J. Sol-Gel Sci. Technol.* **2017**, *84*, 507–514. [[CrossRef](#)]
10. Almeida, C.M.R.; Ghica, M.E.; Durães, L. An overview on alumina-silica-based aerogels. *Adv. Colloid Interface Sci.* **2020**, *282*, 102189. [[CrossRef](#)]
11. Lebedev, A.E.; Menshutina, N.V.; Khudeev, I.I.; Kamyshevsky, R.A. Investigation of alumina aerogel structural characteristics at different «precursor-water-ethanol» ratio. *J. Non-Cryst. Solids* **2021**, *553*, 120475. [[CrossRef](#)]
12. Poco, J.F.; Satcher, J.H.; Hrubesh, L.W. Synthesis of high porosity, monolithic alumina aerogels. *J. Non-Cryst. Solids* **2001**, *285*, 57–63. [[CrossRef](#)]
13. Li, F.B.; Li, M.; Xu, X.; Yang, Z.C.; Xu, H.; Jia, C.K.; Li, K.; He, J.; Li, B.; Wang, H. Understanding colossal barocaloric effects in plastic crystals. *Nat. Commun.* **2020**, *11*, 4190. [[CrossRef](#)]
14. Horiuchi, T.; Chen, L.; Osaki, T.; Sugiyama, T.; Suzuki, K.; Mori, T. A novel alumina catalyst support with high thermal stability derived from silica-modified alumina aerogel. *Catal. Lett.* **1999**, *58*, 89–92. [[CrossRef](#)]
15. Horiuchi, T.; Osaki, T.; Sugiyama, T.; Suzuki, K.; Mori, T. Maintenance of large surface area of alumina heated at elevated temperatures above 1300 °C by preparing silica-containing pseudoboehmite aerogel. *J. Non-Cryst. Solids* **2001**, *291*, 187–198. [[CrossRef](#)]
16. Zu, G.; Shen, J.; Zou, L.; Wang, W.; Lian, Y.; Zhang, Z.; Du, A. Nanoengineering Super Heat-Resistant, Strong Alumina Aerogels. *Chem. Mater.* **2013**, *25*, 4757–4764. [[CrossRef](#)]
17. Xu, X.; Fu, S.; Guo, J.; Li, H.; Huang, Y.; Duan, X. Elastic ceramic aerogels for thermal superinsulation under extreme conditions. *Mater. Today* **2021**, *42*, 162–177. [[CrossRef](#)]
18. Yang, J.; Wang, Q.; Wang, T.; Liang, Y. Facile one-step precursor-to-aerogel synthesis of silica-doped alumina aerogels with high specific surface area at elevated temperatures. *J. Porous Mater.* **2017**, *24*, 889–897. [[CrossRef](#)]
19. Wang, W.; Zhang, Z.; Zu, G.; Shen, J.; Zou, L.; Lian, Y.; Liu, B.; Zhang, F. Trimethylethoxysilane-modified super heat-resistant alumina aerogels for high-temperature thermal insulation and adsorption applications. *RSC Adv.* **2014**, *4*, 54864–54871. [[CrossRef](#)]
20. Zhang, X.; Zhang, R.; Jin, S.; Hu, Z.; Liu, Y.; Jin, M. Synthesis of alumina aerogels from AlCl₃·6H₂O with an aid of acetoacetic-grafted polyvinyl alcohol. *J. Sol-Gel Sci. Technol.* **2018**, *87*, 486–495. [[CrossRef](#)]
21. Wu, X.; Shao, G.; Shen, X.; Cui, S.; Wang, L. Novel Al₂O₃-SiO₂ composite aerogels with high specific surface area at elevated temperatures with different alumina/silica molar ratios prepared by a non-alkoxide sol-gel method. *RSC Adv.* **2016**, *6*, 5611–5620. [[CrossRef](#)]
22. Li, L.; Liu, X.; Wang, G.; Liu, Y.; Kang, W.; Deng, N.; Zhuang, X.; Zhou, X. Research progress of ultrafine alumina fiber prepared by sol-gel method: A review. *Chem. Eng. J.* **2021**, *421*, 127744. [[CrossRef](#)]
23. Yu, H.; Tong, Z.; Yue, S.; Li, X.; Su, D.; Ji, H. Effect of SiO₂ deposition on thermal stability of Al₂O₃-SiO₂ aerogel. *J. Eur. Ceram. Soc.* **2021**, *41*, 580–589. [[CrossRef](#)]
24. Baumann, T.F.; Gash, A.E.; Chinn, S.C.; Sawvel, A.M.; Maxwell, R.S.; Satcher, J.H. Synthesis of High-Surface-Area Alumina Aerogels without the Use of Alkoxide Precursors. *Chem. Mater.* **2005**, *17*, 395–401. [[CrossRef](#)]
25. Wu, X.; Shao, G.; Cui, S.; Wang, L.; Shen, X. Synthesis of a novel Al₂O₃-SiO₂ composite aerogel with high specific surface area at elevated temperatures using inexpensive inorganic salt of aluminum. *Ceram. Int.* **2016**, *42*, 874–882. [[CrossRef](#)]
26. Osaki, T.; Nagashima, K.; Watari, K.; Tajiri, K. Silica-doped alumina cryogels with high thermal stability. *J. Non-Cryst. Solids* **2007**, *353*, 2436–2442. [[CrossRef](#)]
27. Pakharukova, V.P.; Shalygin, A.S.; Gerasimov, E.Y.; Tsybulya, S.V.; Martyanov, O.N. Structure and morphology evolution of silica-modified pseudoboehmite aerogels during heat treatment. *J. Solid State Chem.* **2016**, *233*, 294–302. [[CrossRef](#)]
28. Levin, I.; Brandon, D. Metastable alumina polymorphs: Crystal structures and transition sequences. *J. AM. Ceram. Soc.* **1998**, *81*, 1995–2012. [[CrossRef](#)]
29. Tsukada, T.; Segawa, H.; Yasumori, A.; Okada, K. Crystallinity of boehmite and its effect on the phase transition temperature of alumina. *J. Mater. Chem.* **1999**, *9*, 549–553. [[CrossRef](#)]
30. Boumaza, A.; Favaro, L.; Lédion, J.; Sattonnay, G.; Brubach, J.B.; Berthet, P.; Huntz, A.M.; Roy, P.; Tétot, R. Transition alumina phases induced by heat treatment of boehmite: An X-ray diffraction and infrared spectroscopy study. *J. Solid State Chem.* **2009**, *182*, 1171–1176. [[CrossRef](#)]
31. Li, G.; Liu, Y.; Liu, D.; Liu, L.; Liu, C. Synthesis of flower-like Boehmite (AlOOH) via a simple solvothermal process without surfactant. *Mater. Res. Bull.* **2010**, *45*, 1487–1491. [[CrossRef](#)]

32. Peng, F.; Jiang, Y.; Feng, J.; Li, L.; Cai, H.; Feng, J. A facile method to fabricate monolithic alumina–silica aerogels with high surface areas and good mechanical properties. *J. Eur. Ceram. Soc.* **2020**, *40*, 2480–2488. [[CrossRef](#)]
33. Zu, G.; Shen, J.; Wei, X.; Ni, X.; Zhang, Z.; Wang, J.; Liu, G. Preparation and characterization of monolithic alumina aerogels. *J. Non-Cryst. Solids* **2011**, *357*, 2903–2906. [[CrossRef](#)]
34. Carnes, C.L.; Kapoor, P.N.; Klabunde, K.J.; Bonevich, J. Synthesis, Characterization, and Adsorption Studies of Nanocrystalline Aluminum Oxide and a Bimetallic Nanocrystalline Aluminum Oxide/Magnesium Oxide. *Chem. Mater.* **2002**, *14*, 2922–2929. [[CrossRef](#)]
35. Mei, J.; Yuan, G.; Bai, J.; Ma, Y.; Ren, L. One-pot synthesis of bimetallic catalyst loaded on alumina aerogel as green heterogeneous catalyst: Efficiency, stability, and mechanism. *J. Taiwan Inst. Chem. Eng.* **2019**, *101*, 41–49. [[CrossRef](#)]
36. Sing, K.S.W. Reporting physisorption data for gas/solid systems with special reference to the determination of surface area and porosity. *Pure Appl. Chem.* **1985**, *57*, 603–619. [[CrossRef](#)]

Disclaimer/Publisher’s Note: The statements, opinions and data contained in all publications are solely those of the individual author(s) and contributor(s) and not of MDPI and/or the editor(s). MDPI and/or the editor(s) disclaim responsibility for any injury to people or property resulting from any ideas, methods, instructions or products referred to in the content.